Earth and Planetary Science Letters 286 (2009) 285–291

Contents lists available at ScienceDirect

Earth and Planetary Science Letters

journal homepage: www.elsevier.com/locate/epsl

3D imaging of fracture propagation using synchrotron X-ray microtomography

François Renard [a,b,*], Dominique Bernard [c], Jacques Desrues [d], Audrey Ougier-Simonin [e]

[a] Université Joseph Fourier-Grenoble I, LGCA-CNRS-Observatoire de Grenoble, BP 53, F-38041 Grenoble, France
[b] Physics of Geological Processes, University of Oslo, Norway
[c] Institut de Chimie de la Matière Condensée de Bordeaux, ICMCB-CNRS, 87 avenue du Dr. A. Schweitzer, F-33608 Pessac, France
[d] 3S-R, CNRS-Grenoble Universités, BP 53, F-38041 Grenoble cedex 9, France
[e] Laboratoire de Géologie, Département TAO-Ecole Normale Supérieure, 24 rue Lhomond, 75005 Paris, France

ARTICLE INFO

Article history:
Received 31 July 2008
Received in revised form 18 May 2009
Accepted 26 June 2009
Available online 25 July 2009

Editor: L. Stixrude

Keywords:
X-ray computed microtomography
hydraulic fracture
rupture initiation
fracture propagation

ABSTRACT

During its propagation in a rock a fracture may cross mechanical heterogeneities, which modify the stress field near the crack tip and therefore may affect the direction of propagation. Pre-existing strong (grains) and weak (pores, microcracks) defects control the final path of the fracture and the amplitude of its out-of-plane fluctuations; they may also control rupture arrest. In situ quantification of the role of heterogeneities on fracture propagation is challenging because of the technical difficulty to image the interior of a 3D medium at high spatial resolution. Here, hydraulic tension fractures were produced in 5% porosity limestone core samples, using a specially designed hydraulic cell. The 3D geometry of the centimeter-scale samples was imaged before and after fracturing, using X-ray computed synchrotron microtomography at a voxel resolution of $4.91 \times 4.91 \times 4.91$ μm. The data show that hydraulic fractures propagated by linkage of pores, leading to a macroscopic fracture with well-developed roughness. Moreover, it was possible to estimate that the hydraulic fractures crossed up to 40% more heterogeneities (pores) than if they had propagated into the porous medium by randomly connecting these pores. This demonstrates and quantifies the strong control of local mechanical variations on rupture propagation. A statistical model of fracture propagation is proposed, involving linkage of nearest pores; this model quantitatively reproduces our experimental observation.

1. Introduction

The growth of fractures in rocks under the driving effect of a fluid arises in various geological systems. Natural fracture patterns include intrusive magmatic dykes and sills propagating in the Earth's lithosphere, earthquakes swarms generated by fluid overpressure that also presumably control slow earthquakes and tremor dynamics. Fractures or faults that are driven by a viscous fluid represent a particular class of tensile fractures. They form by the linking of joints or microcracks (Segall and Pollard, 1983). Usually the linkage occurs by formation of arrays of mode I cracks, between linear defects reactivated in shear. This mechanism differs from what is observed for shear fractures that form by the coalescence of microcrack networks (Moore and Lockner, 1995) and where damage releases local stress concentrations in a process zone close to the crack tip (Gonx and Meguid, 1991). The final geometry of the fracture pattern is controlled by the interplay between seepage forces, the size of the injection area, initial stress conditions, and material properties (Rozhko et al., 2007).

Hydrofracturing is also a technique of great importance in soil mechanics and is used systematically to improve oil and gas recovery in low permeability underground reservoirs. For example, hydraulic fracturing has been used to stimulate about 70% of the gas wells and 50% of the oil wells drilled in North America. Other industrial applications involve the extraction of heat in geothermal reservoirs or induced caving in the mining industry. In field hydraulic experiments, depending on the far-field stress, the injection rate and the rock permeability, either shear fracture or tension fracture is the dominant mechanism of hydraulic fracture propagation (Lockner and Byerlee, 1977). As hydraulic extension fractures migrate parallel to the main compressive stress, they can also be used to measure the local main stress direction in the Earth's upper crust (Talebi and Cornet, 1987).

Several models of hydraulic fractures consider a 2D planar fracture plane inside a homogeneous elastic medium (Bunger and Detournay, 2005; Zhang et al., 2005, Garagash, 2006). However, rocks are heterogeneous at all scales and it can be shown that, among other properties, the spatial distribution of the cohesion has a crucial effect on the fracturing pattern. Indeed, discrete simulations using elastic spring networks with disorder demonstrate that hydraulic fracture can acquire fractal geometries, with strong spatial and temporal correlations as the fracture propagates into successive bursts clustered in time (Tzschichholz and Herrmann, 1995). These models could not be tested in laboratory experiments or on in situ observations on natural fractures. However, they showed that heterogeneities in the

* Corresponding author. Université Joseph Fourier-Grenoble I, LGCA-CNRS-Observatoire de Grenoble, BP 53, F-38041 Grenoble, France.
E-mail address: Francois.Renard@ujf-grenoble.fr (F. Renard).

0012-821X/$ – see front matter © 2009 Elsevier B.V. All rights reserved.
doi:10.1016/j.epsl.2009.06.040

fluid flow related to local variations of the permeability can modify the stress field at the fracture tip during its propagation. This indicates that the local 3D geometry in the porous solid may be an important controlling parameter.

A way to visualize a sample in 3D at high resolution is by using 3D X-ray computed tomography. This technique has proven useful in various geophysical and material science problems: imaging of impact breccia (Koeberl et al., 2002) or rock textures (Carlson et al., 1999), characterization of superplastic deformation in metals (Martin et al., 2000), aggregate deformation by pressure solution creep (Renard et al., 2004), shear band deformation in soils (Desrues et al., 1996) or in clay rocks (Lenoir et al., 2007), bubble formation in rhyolitic melts (Okumura et al., 2006), and prediction of permeability from 3D data of porous solids (Bernard et al., 2005; Renard et al., 2006; Fredrich et al., 2006, and references therein).

Here, we have built a small hydraulic fracture cell to generate fractures into porous limestone core samples. We image volumes before and after fracturing, using high resolution X-ray tomography. These 3D data allow isolating the fracture path and characterizing its roughness, based on the initial heterogeneous distribution of pores in the rock. We also propose a simple model of quasi-static fracture propagation that reproduces the effect of initial heterogeneities on the complexity of fracture path. To our knowledge, these 3D measurements in intact rocks and in fractured samples during fluid injection represent new data in the field of fracture mechanics.

2. Hydraulic fractures experiments

A hydraulic cell was especially designed that allowed the control of fracture onset in limestone core samples (Fig. 1). Three samples (Table 1) were drilled in a block of porous limestone extracted from the Anstrude quarry (Burgundy, France). This is an oolitic limestone with 5.2% porosity, a permeability of 3 10^{-15} m^2, and a uniaxial compression strength in the range 30–40 MPa.

In each core sample a hole was carefully drilled along the cylinder axis. The resulting sample was a hollow cylinder with an outer diameter of 9 mm, and a central 2 mm diameter internal hole (Fig. 1a). A first X-ray tomography scan was performed on water saturated samples. Then, the sample was placed between two brass holders into the hydraulic cell (Fig. 1b). Rubber O-rings were used to separate the injection fluid path (fluid inlet, connected to the central hole of the specimen) from the extraction fluid path (lateral chamber connected to the fluid outlet). Another set of O-rings was used to seal the chamber at the piston-holder interface. The sample was free to deform radially. During each experiment, the fluid pressure was slowly increased in the central hole and the flux of water coming out of the sample was monitored with a digital balance. When breakage occurred, the fluid pressure was released and the broken sample was removed from the hydraulic cell for a second tomography scan.

The 3D microtomography data were acquired on beamline ID19 at the European Synchrotron Radiation Facility at a voxel resolution of $4.91 \times 4.91 \times 4.91$ μm under an energy of 25 keV. An X-ray beam was sent onto the sample that was rotated around a vertical axis over a range of 180° in 1000 steps. A series of radiographs was taken using a low-noise 14 bits camera. Based on the sets of projections, a reconstruction algorithm was used to obtain a tomogram representing the 3D microstructure of the sample. Well-contrasted images were obtained, resulting from the difference in X-ray absorption between calcite grains and empty pores (Fig. 2). Because of the large porosity of the fractures and their low X-ray absorption, they can be clearly isolated in the raw scans (Fig. 3a, b).

Quantitative analysis of the tomography data requires separating the pore voxels from the solid ones. This is done using a segmentation procedure that is inherently complicated as some voxels encompass both solid and pore. This effect leads to non-binary data distribution even if a bimodal distribution does exist. An additional image processing artefact is the presence of "ring artefacts" that could be removed using filtering of the sinogram projections (Bernard and Chirazi, 2006). A threshold operation was applied to generate binary 3D images.

In order to highlight the fracture path, the volumes of the two halves of the fractured sample were projected in the initial non fractured sample coordinate system. This projection step first required disconnecting the two halves of the broken sample (Fig. 3c) and processing them separately. In the solid, some denser grains attenuate X-rays more than calcite grains, resulting in high intensity regions in the images. These areas can easily be segmented, and their centres of gravity are precisely located. As a result, a set of reference points was obtained for the unbroken sample and for each half of the broken sample. Using these reference points and an iterative closest points algorithm, it was possible to calculate the translation and solid rotation that superimposes the point set (and thus the microtomograph) of the initial and broken samples (Fig. 3d). Using this technique it was possible to localise with precision the path followed by the fracture.

Fig. 4 shows the topography of the two fractures that propagated from the central hole in sample ANS2SC. The fractures have connected the pores, and propagated mainly by breaking the cement between the grains (Fig. 5). Note also that some grains have been broken. The final topography of the fracture is then strongly dependent on this mechanism of propagation. The large rounded peaks and pits in Fig. 4 correspond to grains that were avoided by the fracture. As these grains were surrounded by pores (white patches in Fig. 4), the fracture propagated by linkage of these weak parts of the porous matrix. We also checked that no pre-existing microcracks could be detected in the samples and could have acted as privileged fracturing nucleation sites. This observation does not rule out the possibility that microcracks, not detectable due to the limited resolution of the X-ray measurements, could have controlled fracture propagation. However, we will see below that we can explain the micromechanics of hydraulic fracture propagation without involving an additional effect of such microcracks.

The result is a rough fracture, whose roughness exponent could be estimated using a box counting method (Schmittbuhl et al., 1995) and found to be close to 0.80 ± 0.10 for the data shown in Fig. 5. However, the high level of noise in the data make this number difficult to compare with existing models of fracture roughness exponents (Bouchaud et al., 2002). Finally, it is worth mentioning that the core sample broke in two pieces, with an angle between the fractures close to 180° (Table 1), whereas other experiments at higher confining stress indicate that, for such cylindrical geometry, the sample usually breaks in 3 parts with 120° angles (Vinciguerra et al., 2004).

The effect of initial heterogeneities on the fracture path can be characterized by counting how many pores the fractures had connected, and compare this value to the actual porosity of the sample. One can define the fracture porosity ϕ_{frac} as the number of pore pixels in the fracture, divided by the number of fracture pixels. An excess fracture porosity can then be calculated as $\phi_{ex} = (\phi_{frac} - \phi_0)/\phi_0$, where ϕ_0 is the rock porosity (see Table 1). Our data show that the fractures contain 16% to 41% more porosity than a random slice in the rock with the same roughness amplitude as the fractures. This demonstrates that the fracture did not propagate straightly in the direction perpendicular to the maximum tensile stress, but was perturbed by local structural heterogeneities. The value of the excess porosity should therefore depend on the amount and spatial distribution of the mechanical heterogeneities initially present in the rock.

3. Stochastic model of fracture propagation into a heterogeneous medium

Scholz (1968) proposed that, in a stressed rock volume, heterogeneity leads to local stresses whose magnitudes deviate significantly from that of the applied stress. The volume of the rock can be divided

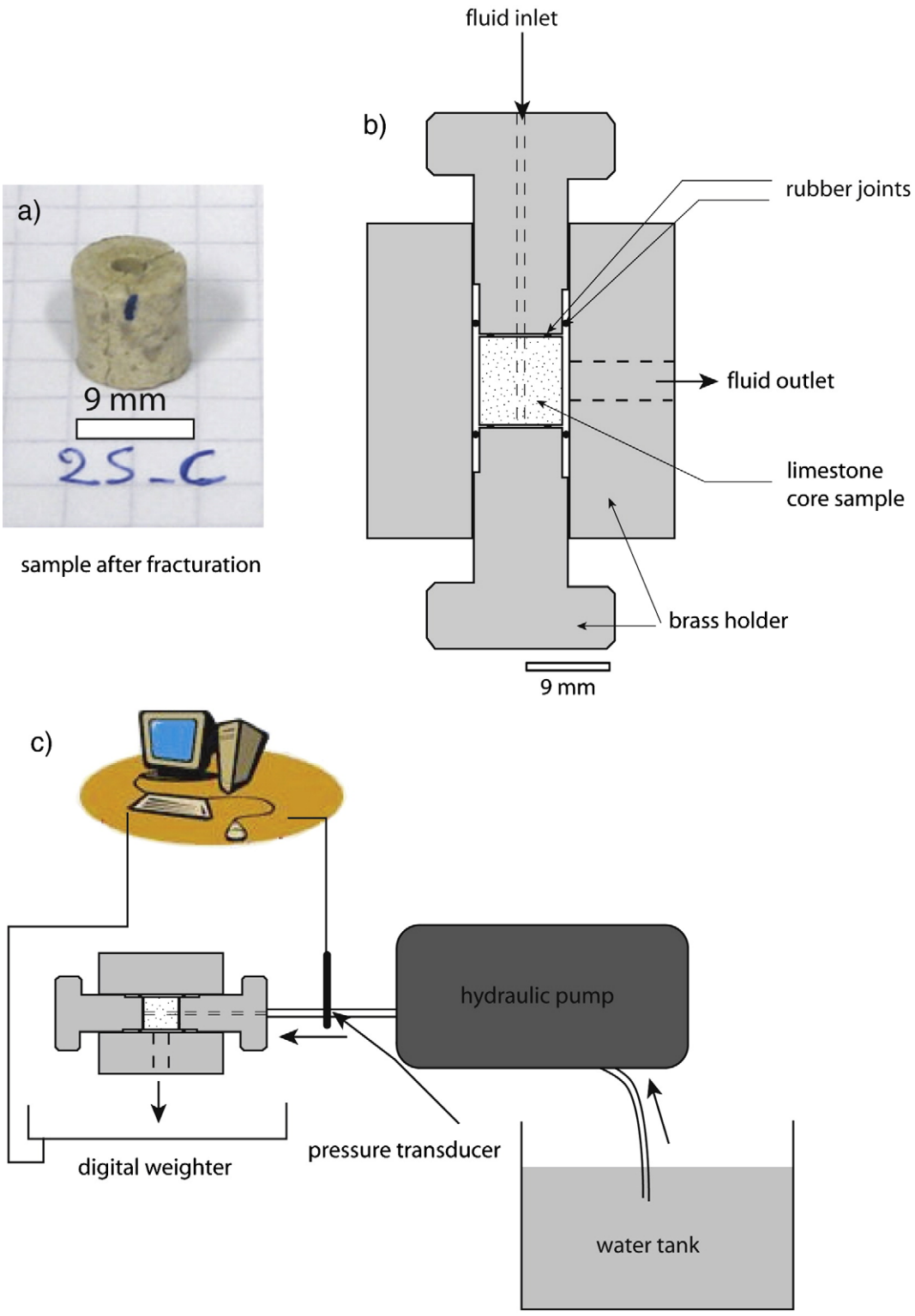

Fig. 1. a) Limestone core sample Anstrude2SC after fracturing. The cylindrical sample is 9 mm wide, with a 2 mm diameter hole in its center. b) Miniature hydraulic fracturing cell. c) Experimental set-up.

into small regions each possessing a specific strength and, when the local stress reaches the local strength, the region fails leading to the propagation of the crack. This crack may be arrested if it enters a region of higher strength or lower local stress. Heterogeneities affect the roughness of the fracture surface by inducing random mode II loading on the crack front as the crack grows and relieves the residual stresses (Ramanathan et al., 1997; Bouchaud et al., 2002). The presence of heterogeneities will make the crack curve in the direction in which the "hoop stress" (tangential stress) or total stress is larger and the crack will tend to bend in the direction of lower yield stress (i.e., pores) (Ramanathan et al., 1997). Defects may therefore be regarded as stress concentrators, and accorded an appropriate importance in controlling

Table 1
Table of experiments.

Sample #	Fluid pressure at fracturing (MPa)	Angle between the fractures	Tomography acquisition	Rock porosity	Fracture porosity	Excess porosity
Anstrude1SC	2.72	154°	No	–	–	–
Anstrude2SC	3.18	162°	Yes	5.2%	7.1% 7.4%	36% 41%
Anstrude4MC	0.97	178°	Yes	5.2%	6.2% 7.0%	18% 33%

fracture propagation. In our experiments, such heterogeneities correspond to pore or grain boundaries, in other rocks it could also correspond to pre-existing micro cracks.

At least two kinds of numerical models have been proposed to reproduce damage and fracture propagation in rocks: the continuum approach and the discrete/stochastic models based on fracture

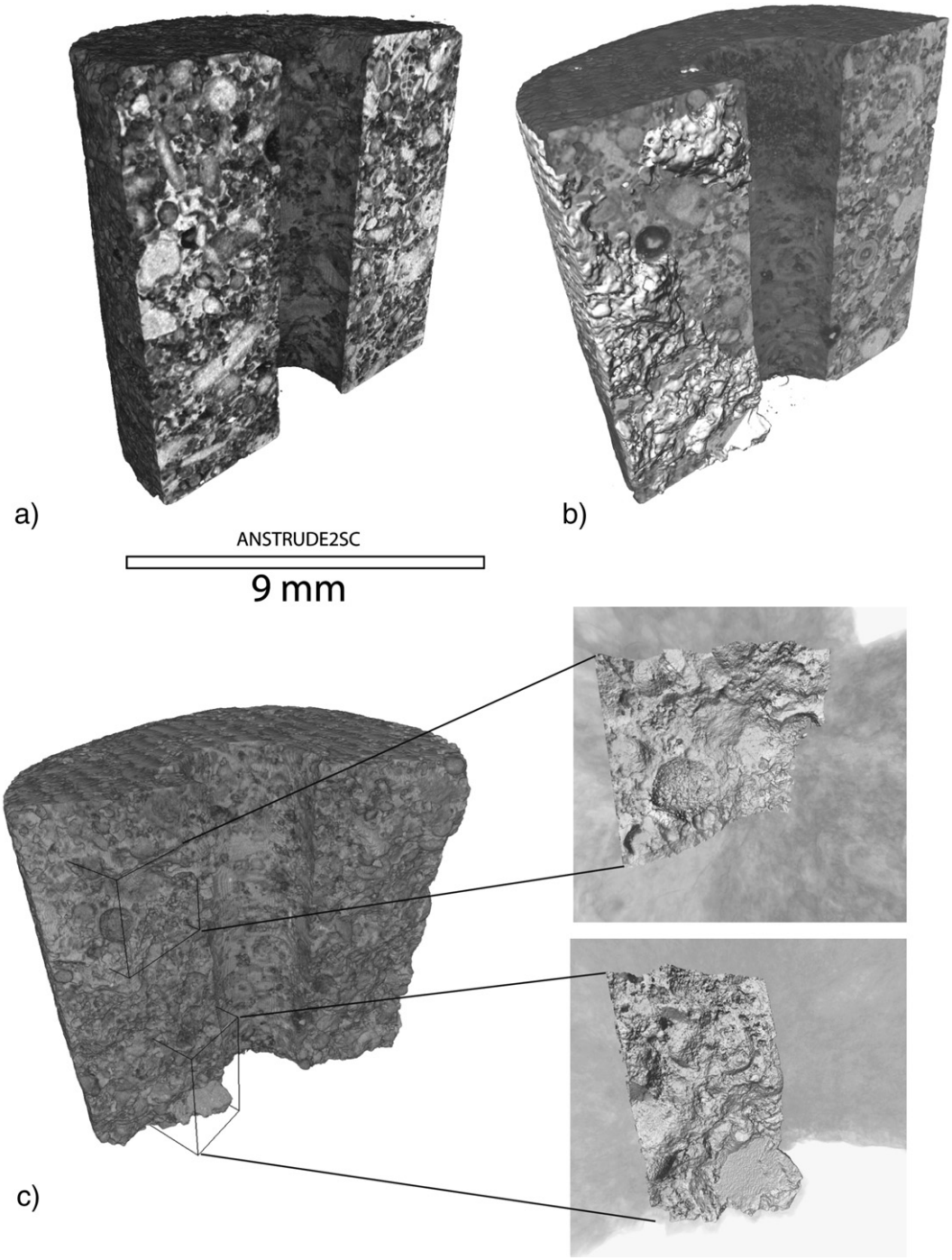

Fig. 2. Microtomography data: 3D views of sample ANSTRUDE2SC before and after fracturing. a) Sample before fracturing, where half of the sample is displayed, showing individual grains and the central hole where fluid injection was performed. b) Same sample after fracturing, showing the fracture fluctuating around a flat plane. c) Zoom on the fracture surface, where rounded shapes indicate that the fracture did propagate around individual grains.

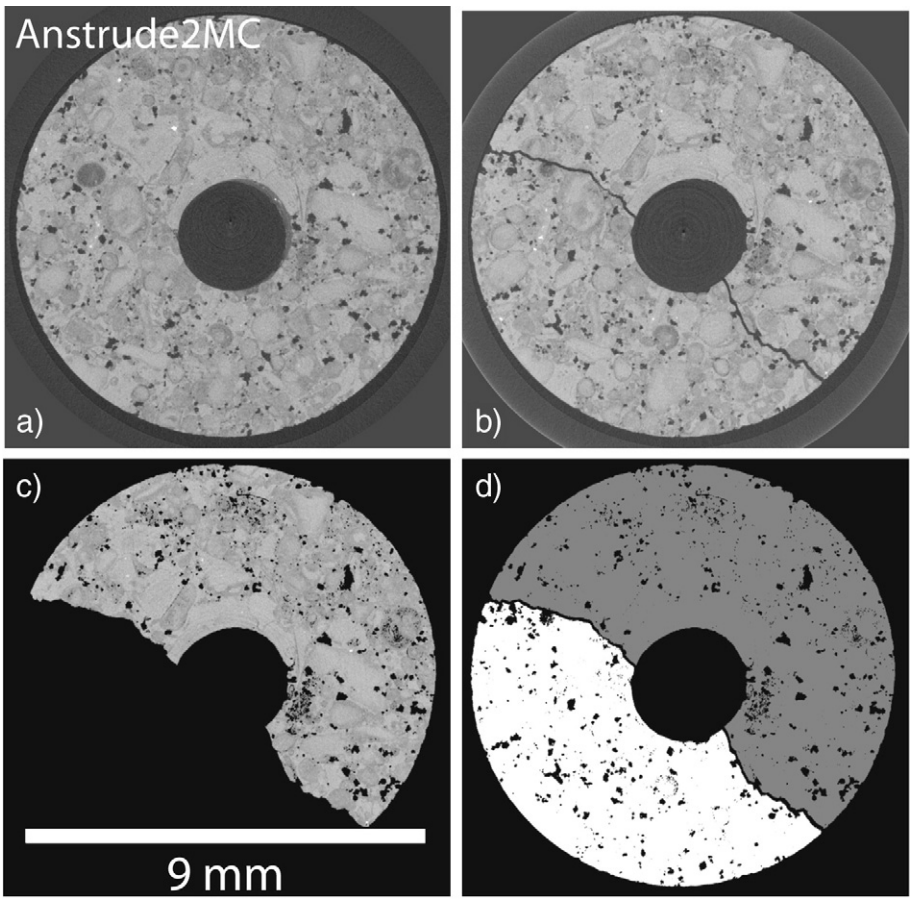

Fig. 3. Microtomography data. 2D sections in sample Anstrude2MC before (a) and after (b) fracturing. The gray levels measure the amount of X-ray absorption, showing the porosity in dark and calcite grains in light gray. c) Separation of one broken fragment and projection into the same 3D coordinate system as the sample before fracturing. d) Segmentation of the data to separate the solid matrix from the porosity and locate the fracture.

micromechanics. Continuum finite element models of circular holes under internal hydraulic pressure were performed by Yang et al. (2004). They took into account the coupling between stress processes and seepage forces, and showed that the roughness of the fracture path and the breakdown pressure were considerably influenced by the mechanical heterogeneities initially present in the rock. The presence of randomly assigned heterogeneities induced significant shear and normal stress variations away from the crack tip, that were large enough to control the quasi-static propagation of the hydraulic

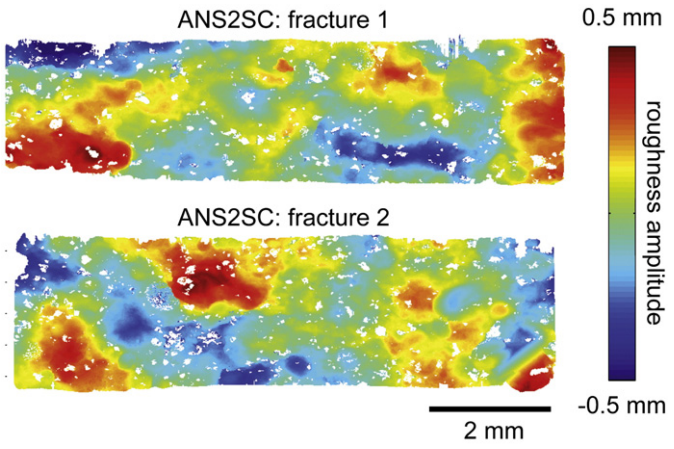

Fig. 4. Topography of the two fracture branches extracted from the 3D data in sample ANS2SC. The roughness amplitude is represented by the colour scale, whereas the pores that were crossed by the fracture are left in white.

fractures. Using a linear elastic fracture mechanics approach, Fond et al. (1995) have calculated analytically how the presence of heterogeneities in the medium modifies its elastic properties. They demonstrated that the presence of pores that interact elastically in the solid may reduce the elastic domain by up to 30% in the tensile region and that elastic crack interactions can render a solid stiffer than in a system with no interaction. Blair and Cook (1998) decomposed the stress field in a cracked rock into one of an elastic continuum and one of a cracked elastic body. Strength heterogeneity was introduced by assigning different tensile strength values to different sites, with stress heterogeneity being simulated by the introduction of a perturbation to the continuum stress field. Although the model was based on linear approximation, it produced a non-linear response.

Numerical models of fracture propagation and progressive mechanical breakdown, based on a discrete network approach have proved popular, because such lattice-type models consist of fewer unknowns and are computationally more economical than continuum models. Such models can reproduce strain localization in heterogeneous solids and the coupling with fluid transport (Yuan and Harrison, 2006) or the complex pattern of microcrack coalescence and fracture roughness development (Tzschichholz et al., 1994). However, they rely on a prescribed porous solid geometry, which is usually randomly chosen with statistical distribution and correlation of mechanical heterogeneities. The comparison with a natural fracture has, to our knowledge, not been performed yet because of the lack of high resolution reliable 3D data.

To estimate how the excess porosity observed in the experiments depends on the initial rock porosity, we model fracture propagation using the fact that, under external stress, stresses intensify around

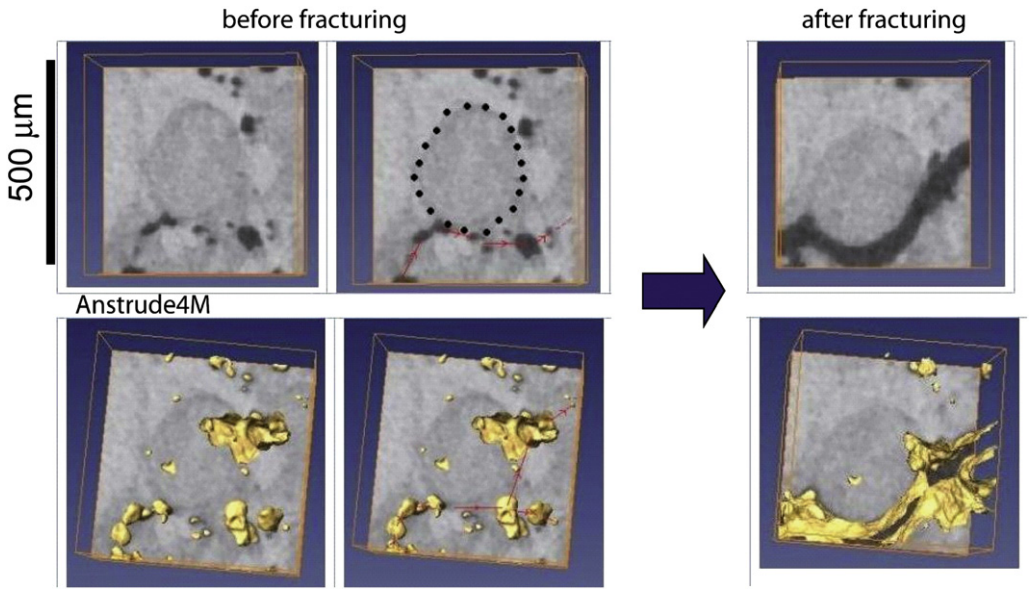

Fig. 5. Propagation of the fracture inside the volume (left: before fracturing, middle: fracture path drawn, right: after fracturing). The fracture has propagated by connecting pores (dark) and avoiding hard grains (light gray levels, surrounded by the dashed line), providing an explanation why more pores are connected by the fracture than a random surface in the volume. The bottom raw displays the angular shape of the pores.

the pores, with tensile components developing on the boundary of the pore. As a result, tensile cracks are induced on the boundary of the pore, in a direction parallel, or inclined at a small angle, to the direction of maximum stress (Sammis and Ashby, 1986; Yuan et al., 1993). Since most materials crack under tension and in much less degree under compression, we assume that the hydraulic fractures

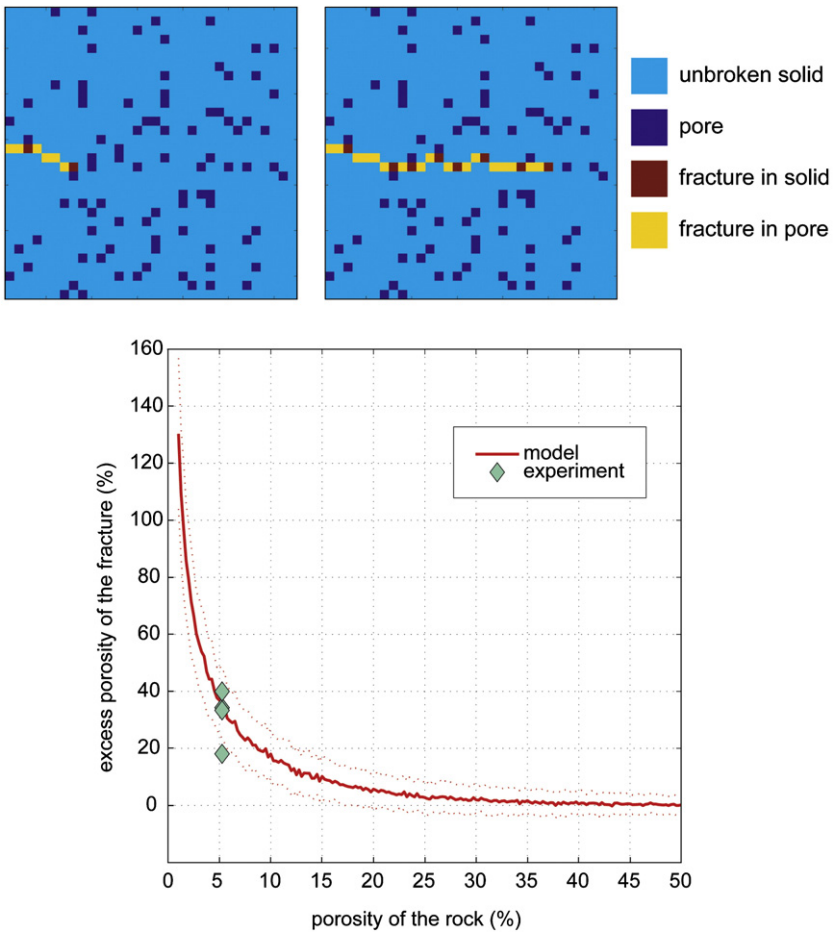

Fig. 6. Discrete model of fracture propagation into a heterogeneous porous medium. Top: the fracture propagates by increments, from the left to the right, and connects nearest pores. Bottom: excess porosity of the fracture compared to the initial porosity of the rock. The model (red thick line: average of 100 simulations, red dotted lines: one standard deviation) and the data of the four experimental fractures are also represented.

propagated by successive increments under tension, as observed using acoustic emission records (Vinciguerra et al., 2004; Al-Busaidi et al., 2006).

A simple discrete model of fracture propagation in two-dimensions was developed (Fig. 6). Firstly, a 2D square porous medium, with a known porosity was built, where each pixel had a probability ϕ_0 to be a pore and a probability $(1-\phi_0)$ to be a solid. We consider here that pores and grains have the same size. Here, ϕ_0 represents the porosity of the medium. Secondly, a notch was defined in the middle of the left hand side of the square porous medium, and a uniaxial vertical tensile stress was applied to the system. Thirdly, a simple rule was defined for quasi-static fracture propagation by successive increments: the tensile stress was calculated at the notch tip and at each pore, using the stress intensity factor for tensile cracks. We consider here that each pore represents a flaw in the porous medium. Then all the stress perturbations due to the fracture tip and the pores were added, assuming that their individual contributions are linear. Finally, a fracture increment was defined by breaking the solid between the notch tip and the pore where stress concentration was the highest (Fig. 6). This model aims at reproducing the experimental observation of pore connection during fracture propagation (Fig. 5).

Using this discrete model, we can calculate the amount of pores the fracture crosses during propagation and calculate the excess porosity of the fracture as a function of the initial rock porosity (Fig. 6). As each simulation of the model depends on the initial porosity distribution, we have performed one hundred simulations on 1024×1024 lattices. The fracture excess porosity is quite large for low porosity rocks (up to 100% for 2% porosity) and decreases almost exponentially to zero for rock porosity close to 45%. Interestingly, the four fractures obtained experimentally fall in the range of excess porosity calculated by the model.

4. Conclusion

Using X-ray microtomograph imaging we have performed a series of hydraulic fracture experiments and showed the strong effect of initial heterogeneities on fracture propagation and final roughness. A rock is typically heterogeneous as it contains initial defects such as grain boundaries, microcracks and pores. In our experiment, the fractures clearly propagated by linkage of existing cavities and grain boundaries (the presence of pre-existing micro cracks could not be demonstrated). The out-of-plane roughness was controlled partly by such heterogeneities and the excess porosity of the fracture may attain 40%. Our discrete model of fracture propagation by linkage of nearest pores reproduces this property.

Continuum numerical simulations based on the deformation of a heterogeneous elastic solid under the effect of a pressure gradient should represent a future task for fracture propagation prediction. High-resolution microtomography imaging is a powerful technique to acquire such data and will open a new era in realistic 3D mechanical modeling of complex processes in heterogeneous media such as geomaterials.

Acknowledgments

The authors would like to thank Elodie Boller at ESRF, Robert Guiguet at LGIT for designing the hydraulic cell, and Christophe Rousseau at 3 S-R for designing the data acquisition software and managing the hydraulic load control system during the tests.

References

Al-Busaidi, A., Hazard, J.F., Young, P., 2006. Distinct element method of hydraulically fractured Lac du Bonnet granite. J. Geophys. Res. 110, B06302. doi:10.1029/2004JB003297.

Bernard, D., Chirazi, A., 2006. Numerically enhanced microtomographic imaging method using a novel ring artefact filter. In: Desrues, J., Viggiani, G., Bésuelle, P. (Eds.), Advances in X-ray tomography for geomaterials. ISTE, London. ISBN: 1 905209 60 6, pp. 119–124.

Bernard, D., Nielsen, O., Salvo, L., Cloetens, P., 2005. Permeability assessment by 3D interdentritic flow simulations on microtomography mappings of Al–Cu alloys. Mater. Sci. Eng. A 192, 112–120.

Blair, S.C., Cook, N.G.W., 1998. Analysis of compressive fracture in rock using statistical techniques: Part I. A non-linear rule-based model. Int. J. Rock. Mech. Min. Sci. 35, 837–848.

Bouchaud, E., Bouchaud, J.P., Fisher, D.S., Ramanathan, S., Rice, J.R., 2002. Can crack front waves explain the roughness of cracks? J. Mech. Phys. Solids 50, 1703–1725.

Bunger, A.P., Detournay, E., 2005. Asymptotic solution for a penny-shaped near-surface hydraulic fracture. Eng. Fract. Mech. 72, 2468–2486.

Carlson, W.D., Denison, R., Ketcham, R.A., 1999. High-resolution computed tomography as a tool for visualization and quantitative analysis of igneous textures in three dimensions. Electron. Geosci. 4, 3.

Desrues, J., Chambon, R., Mokni, M., Mazerolle, F., 1996. Void ratio evolution inside shear bands in triaxial sand specimens studied by computed tomography. Geotechnique 46, 529–546.

Fond, C., Flejou, J.L., Berthaud, Y., 1995. Interactions between cracks and circular holes in two-dimensional linear elastic media. Eur. J. Mech. A, Solids 14, 73–96.

Fredrich, J.T., Di Giovanni, A.A., Noble, D.R., 2006. Predicting macroscopic transport properties using microscopic image data. J. Geophys. Res. 111, B03201. doi:10.1029/2005JB003774.

Garagash, D.I., 2006. Plane-strain propagation in a fluid-driven fracture during injection and shut-in: asymptotics of large toughness. Eng. Fract. Mech. 73, 456–481.

Gonz, S.Z.X., Meguid, S.A., 1991. On the effect of the release of residual stresses du to near-tip microcracking. Int. J. Fract. 52, 257–274.

Koeberl, C., Denison, C., Ketcham, R.A., Reimold, W.U., 2002. High-resolution X-ray computed tomography of impactites. J. Geophys. Res. 82, 2018–2026.

Lenoir, N., Bornert, M., Desrues, J., Bésuelle, P., Viggiani, G., 2007. Volumetric digital image correlation applied to X-ray microtomography images from triaxial compression tests on argillaceous rock. Strain 43, 193–205.

Lockner, D., Byerlee, J.D., 1977. Hydrofracture in Weber sandstone at high confining pressure and differential stress. J. Geophys. Res. 107 (E10), 5089. doi:10.1029/2001JE001883.

Martin, C.F., Josserond, C., Salvo, L., Blandin, J.J., Cloetens, P., Boller, E., 2000. Characterization by X-ray micro-tomography of cavity coalescence during super-plastic deformation. Scr. Mater. 42, 375–381.

Moore, D.E., Lockner, D.D.A., 1995. The role of microcracking in shear-fracture propagation in granite. J. Struct. Geol. 17, 95–114.

Okumura, S., Nakaùura, M., Tsuchiyama, A., 2006. Shear-induced bubble coalescence in rhyolitic melts with low vesicularity. Geophys. Res. Lett. 33, L20316. doi:10.1029/2006GL027347.

Ramanathan, S., Ertas, D., Fisher, D.S., 1997. Quasistatic propagation in heterogeneous media. Phys. Rev. Lett. 79, 873–876.

Renard, F., Bernard, D., Thibault, X., Boller, E., 2004. Synchrotron 3D microtomography of halite aggregates during experimental pressure solution creep and evolution of the permeability. Geophys. Res. Lett. 31, L07607. doi:10.1029/2004GL019605.

Renard, F., Bernard, D., Desrues, J., Plougonven, E., Ougier-Simonin, A., 2006. Characterization of hydraulic fractures in limestones using X-ray microtomography. In: Desrues, J., Viggiani, G., Bésuelle, P. (Eds.), Advances in X-ray tomography for geomaterials. ISTE, London. ISBN: 1 905209 60 6, pp. 221–227.

Rozhko, A., Podladchikov, Y.Y., Renard, F., 2007. Failure patterns caused by localized rise in pore-fluid overpressure and effective strength of rocks. Geophys. Res. Lett. 34, L22304. doi:10.1029/2007GL031696.

Sammis, C.G., Ashby, M.F., 1986. The failure of brittle porous solids under compressive stress states. Acta Metall. 34, 511–526.

Scholz, C.H., 1968. Experimental study of the fracturing process in brittle rocks. J. Geophys. Res. 88, 555–568.

Schmittbuhl, J., Vilotte, J.P., Roux, S., 1995. Reliability of self-affine measurements. Phys. Rev. E 51, 131–147.

Segall, P., Pollard, D.D., 1983. Nucleation and growth of strike slip faults in granite. J. Geophys. Res. 73, 1447–1454.

Talebi, S., Cornet, F.H., 1987. Analysis of the microseismicity induced by a fluid injection in a granitic rock mass. Geophys. Res. Lett. 14, 227–230.

Tzschichholz, F., Herrmann, H.J., 1995. Simulations of pressure fluctuations and acoustic emission in hydraulic fracturing. Phys. Rev. E 51, 1961–1970.

Tzschichholz, F., Herrmann, H.J., Roman, H.E., Pfuff, M., 1994. Beam model for hydraulic fracturing. Phys. Rev. B 49, 7056–7059.

Vinciguerra, S., Meredith, P.G., Hazzard, J., 2004. Experimental and modelling study of fluid pressure-driven fractures in Darley Dale sandstone. Geophys. Res. Lett. 31, L09609. doi:10.1029/2004GL019638.

Yang, T.H., Tham, L.G., Tang, C.A., Liang, Z.Z., Tsui, Y., 2004. Influence of heterogeneity of mechanical properties on hydraulic fracturing in permeable rocks. Rock Mech. Rock Eng. 37, 251–275.

Yuan, S.C., Harrison, J.P., 2006. A review of the state of the art in modelling progressive mechanical breakdown and associated fluid flow in intact heterogeneous rocks. Int. J. Rock Mech. Min. Sci. 43, 1001–1022.

Yuan, Y.G., Lajtai, E.Z., Ayari, M.L., 1993. Fracture nucleation from a compression-parallel, finite-width elliptical flaw. Int. J. Rock Mech. Min. Sci. Geomech. Abstr. 30, 873–876.

Zhang, X., Jeffrey, R.G., Detournay, E., 2005. Propagation of a hydraulic fracture parallel to a free surface. Int. J. Numer. Anal. Methods Geomech. 29, 1317–1340.